LARGE-EDDY SIMULATION STUDY OF TURBULENT MIXING IN A T-JUNCTION

A.K. Kuczaj[*] **E.M.J. Komen**

Computational Fluid Dynamics, Safety & Performance,
Nuclear Research and Consultancy Group (NRG),
P.O. Box 25, 1755 ZG Petten, The Netherlands

Abstract
A potential cause of thermal fatigue failures in energy cooling systems is identified with cyclic stresses imposed on a piping system. These are generated due to temperature changes in regions where cold and hot flows are intensively mixed together. A typical situation for such mixing appears in turbulent flow through a T-junction, which is investigated here using Large-Eddy Simulations (LES). In general, LES is very well capable in capturing the mixing phenomena and accompanied turbulent flow fluctuations in a T-junction. An assessment of the accuracy of LES predictions is made for the Vreman model through a direct comparison with available experimental results. The integral and Taylor length scales were used to provide the accuracy assessment and error quantification in perfomed simulations. It is shown that the mesh resolution with the average cell-sizes three times smaller than the Taylor microscale length is sufficient to give very similar results to these obtained on much finer meshes. This may serve as an initial engineering guideline for construction of computational meshes that allow for an accurate prediction of turbulent mixing. Additionally, detailed analysis of the temperature measurement data at specified probe locations is presented along with a quantification of an error introduced by LES modelling.

1 INTRODUCTION

Turbulent mixing in nuclear reactor cooling systems can potentially lead to appearance of the thermal fatigue phenomena (Chapuliot *et al.*, 2005). This stimulates development and validation of modelling approaches for turbulent mixing in order to supply detailed information about the amplitudes and frequencies of the flow temperature fluctuations. Usual strategy applied to thermal fatigue prediction involves Computational Fluid Dynamics simulations to determine the temperature fluctuations, which serve as an input for the structural mechanics analyses. Turbulent mixing of hot and cold fluid streams in a T-junction is a challenging test case for such validation. Accurate flow predictions require considerably high computational effort due to a number of scales that need to be resolved in order to capture the nonlinear effects of small-scale flow-structures on the large-scale flow.

In literature, a number of numerical experiments in mixing T-junctions can be found (see (Hu & Kazimi, 2006) and references therein). Simulations with five different physical situations and two configurations of T-junctions were presented in (Hu & Kazimi, 2006). This benchmark study of high cycle temperature fluctuations showed the applicability of LES in prediction of turbulent flow features in a T-junction. Similar conclusions were drawn in (Coste *et al.*, n.d.), where an influence of secondary flow on temperature averages and fluctuations is demonstrated. The secondary flow was imposed by an additional elbow attached to one of the T-junction legs. Simulations with the standard and dynamic Smagorinsky models were compared in (Merzari & Ninokata, n.d.). An advantage of the dynamic model over the Smagorinsky method was shown, because the dynamic procedure better resolves the small-scale turbulence scales as expected due to its less dissipative

[*]Phone: +31 22-456-8045, fax: +31 22-456-8490, e-mail: kuczaj@nrg.eu

character. The utility of both models application for predictions of the mean flow features was demonstrated. Detailed validation is still needed to determine the accuracy and range of validity of applied numerical methods with respect to this subject.

Here, we investigate and assess the accuracy of an LES model applied for modelling of turbulent mixing in a T-junction. There are two main objectives in this paper. *The first one is to determine accuracy of LES predictions for mixing in a T-junction. The second one is to provide an engineering guideline for required computational mesh resolution.*

In such mock-up, two perpendicular streams of flow with different temperatures are mixed together. In this paper, we consider recently developed model by Vreman (Vreman, 2004), which was particularly design for shear dominated flows. We pay special attention to magnitude and frequency of fluctuations that are particularly of great importance for thermal fatigue predictions. Comparison with experimental data provides a conclusive opportunity for assessing a suitability of considered model in prediction of turbulent mixing (Andersson *et al.*, 2006). The experiment presented in (Andersson *et al.*, 2006) was particularly designed to investigate thermal mixing in a T-junction with prescribed flow conditions. By performing simulations with different mesh resolution, we pay special attention to the resolution that need to be used for accurate flow predictions and mesh independent numerical solutions. We will show that large differences occur in predictions of turbulence quantities (mean and fluctuations) that are obtained on the basis of the same LES model but with under-resolved mesh resolution conditions.

The organization of this paper is as follows. In section 2 we introduce the experimental and computational setup. The main objectives are presented in section 3, which is devoted to verification of the applicability of applied modelling method and its numerical validation through a direct comparison with the experiment. In section 4 we provide analysis of the temperature fluctuations. Concluding remarks are collected in section 5.

2 EXPERIMENTAL AND COMPUTATIONAL SETUP

The experimental setup prepared to provide experimental data used for a validation of the mixing process is described in details in (Andersson *et al.*, 2006). It consists of two perpendicularly connected pipes with diameters of $2r_h = 0.1$m (hot flow: z-direction, vertical) and $2r_c = 0.14$m (cold flow: x-direction, horizontal), which form the considered T-junction. In the experiment, the approximate cold and hot flow rates are 12 and and 6l/s. They give average inlet velocity values of $0.76 - 0.78$m/s. Temperature difference between the hot and the cold fluid was set to 15 degrees with $T_h = 303$K and $T_c = 288$K. Temperature fluctuations near the pipe walls have been measured with thermocouples, and the velocity profiles in the inlet pipes and downstream of the T-junction were measured with the Laser Doppler Velocimetry (LDV). The mixing process has also been studied with the Laser Induced Fluorescence (LIF), in which the mixing of a passive scalar was measured by means of concentration. Together, these measurements give sufficiently detailed description of the flow characteristics. For further experimental details we refer to (Andersson *et al.*, 2006). Additionally, flow measurements three diameters upstream from the center of the T-junction for both legs allow to set the inflow conditions for the numerical simulations that are described next.

In our numerical model, we solve the filtered incompressible Navier-Stokes equations, which have the following form (Fureby *et al.*, 1997; Weller *et al.*, 1998):

$$\frac{\partial \overline{\mathbf{u}}}{\partial t} + \nabla \cdot (\overline{\mathbf{u}} \otimes \overline{\mathbf{u}}) + \frac{1}{\rho}\nabla \overline{p} = -\nabla \cdot (\mathbf{B} - 2\nu \mathbf{D}), \tag{1}$$

where $\overline{\mathbf{u}}$ is the filtered velocity with its components (u, v, w) correspondingly in x, y, z direction, $\overline{p}$ is the filtered pressure, and ρ is the fluid density. The symmetric deformation tensor $\mathbf{D}$ is defined as $\mathbf{D} = \frac{1}{2}(\nabla\overline{\mathbf{u}} + \nabla\overline{\mathbf{u}}^T)$ and the subgrid-scale (SGS) stress tensor is $\mathbf{B} = \overline{\mathbf{u} \otimes \mathbf{u}} - \overline{\mathbf{u}} \otimes \overline{\mathbf{u}}$. Usually, the SGS stress tensor $\mathbf{B} = \mathbf{B}_D + \frac{2}{3}k\mathbf{I}$ is parameterized with $k = \frac{1}{2}tr(\mathbf{B})$ and $\mathbf{B}_D$, which is the deviatoric part of $\mathbf{B}$ modelled using an eddy-viscosity assumption: $\mathbf{B}_D = -2\nu_t \mathbf{D}_D$ with respect to the deviatoric part of the deformation tensor $\mathbf{D}_D$. This way, we arrive to a situation, in which k and ν_t must be specified in order to mathematically close these equations. In performed simulations, the recently

developed LES subgrid model by Vreman (Vreman, 2004) was implemented. Comparison of the application of this model with results obtained with the classical Smagorinsky models can be found in (Kuczaj *et al.*, n.d.). This eddy-viscosity model is based on the computation of the turbulence viscosity:

$$\nu_t = \frac{5}{2} C_s^2 \Delta^2 \sqrt{\frac{inv_2(\boldsymbol{\alpha}^T \cdot \boldsymbol{\alpha})}{tr(\boldsymbol{\alpha}^T \cdot \boldsymbol{\alpha})}}, \tag{2}$$

where $\boldsymbol{\alpha} = \nabla \overline{\mathbf{u}}$ and $k = 2\sqrt{2}\nu_t |\mathbf{D}_D|$. The second invariant of the velocity gradients product is denoted by $inv_2(\boldsymbol{\alpha}^T \cdot \boldsymbol{\alpha})$. This formulation is consistent with Eqs. (5-8) in the original paper (Vreman, 2004). The accuracy of this new subgrid model will be determined in the next section.

The Navier-Stokes equations (1) are solved along with a passive scalar equation in the following form:

$$\frac{\partial \overline{T}}{\partial t} + \overline{\mathbf{u}} \cdot \nabla \overline{T} = \Big(\frac{\lambda}{\rho C_p} + \frac{\nu_t}{Pr_t} \Big) \nabla^2 \overline{T}, \tag{3}$$

where $\overline{T}$ is the filtered scalar, $\lambda = 0.6$ $[kg \cdot m/(s^3 \cdot K)]$ is the heat capacity, $C_p = 4.18 \cdot 10^3$ $[m^2/(s^2 \cdot K)]$ is the specific heat and $Pr_t = 0.85$ is the turbulent Prandtl number. The other parameters used in the simulations are density $\rho = 10^3$ $[kg/m^3]$ and laminar viscosity $\nu = 1.005 \cdot 10^{-6}$ $[m^2/s]$. The system of equations (1),(3) along with the incompressibility constraint is solved with a second-order discretization scheme both in space and time. The code is based on standard numerical libraries (Weller *et al.*, 1998), which were developed to solve LES with an additional passive scalar equation. In detail, a second-order backward-differencing based on the current and two previous time-step values is used. The preconditioned (bi-)conjugate gradient method is used for the discretized flow-equations with second-order laplacian, gradient or convection schemes and Gauss' theorem applied for the spatial derivatives. Pressure is eliminated by solving the Poisson equations with PISO velocity-pressure coupling algorithm. For keeping stability of numerical solutions, the simulation time-step is dictated by the CFL condition with a Courant number in the range of 0.7-0.85.

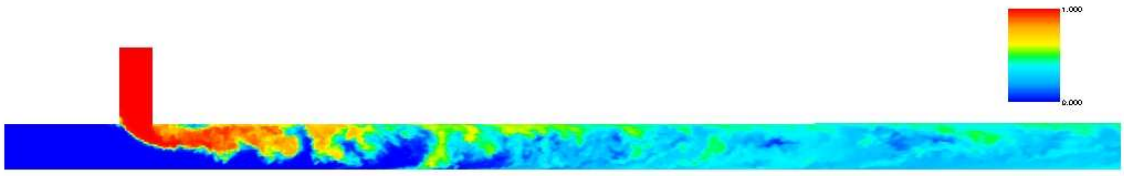

Figure 1: Instantaneous snapshot of the temperature field captured at $t = 12s$ computed on the 2mm mesh.

In the numerical model, the measured velocity profiles as the inflow conditions were used. Geometrical length of the T-junction is 25 diameters (3.5m) in x-direction, with a center of the mixing zone three diameters (0.42m) from the cold inflow. In z-direction the hot leg has length of 3.1 diameters (0.31m) measured from the hot inflow to the center of the mixing zone. The last measurement location is situated two diameters upstream from the outflow. For the prescribed flow conditions, the main generation of turbulence is caused by the mixing of the two fluid streams. This was verified in our test simulations and it was also found in (Westin *et al.*, n.d.). Hence, no perturbation of the inflow velocity conditions was applied.

We perfomed our simulations with a sequence of fully hexahedreal meshes with an average cell-size of 8, 6, 4, 3, and 2mm, to which we will refer further in this text. The corresponding numbers of hexahedral cells are 156.784, 329.508, 949.941, 2.110.810, and 7.286.288 for the finest mesh. This was required to obtain grid-independent numerical results and to determine the accuracy of the numerical predictions. As the direct simulations towards walls are impossible due to small scales that exist in the flow near boundaries, another important aspect is a treatment of the boundary layer. We applied standard wall functions in the formulation similar to Werner and Wengle. For

the prescribed flow conditions, the value of $y^+ \approx 30$ approximately corresponds to 3mm near-wall distance. This near-wall mesh-size value was used for all simulations, apart from the 2mm mesh, where 2mm near-wall mesh size was used. We considered incompressible flow conditions with adiabatic wall treatment, which is a good representation of the flow conditions in the experimental setup. In the next section, validation of computational results based on the experimental data will be given.

3 FlOW CHARACTERISTICS ASSESSMENT

Numerical simulations were performed for the physical time of 12s. Results for the first 5s were neglected due to development of the mixing. This time approximately corresponds to the two-cycle time period needed for the flow to reach the outlet starting from the inlets. Inspection of the temperature measurements near the outflow shows that this transition period is sufficiently long. All time-averages presented in this section are taken for the remaining 7s of the physical time. We also performed computation for the physical time of 30s for the 4mm mesh (25s of averaging time), finding no significant difference in the time-averaged results when compared with these averaged only for 7s. We concluded that 12s of simulation time is sufficiently enough to capture relevant statistics of the flow. This will be also shown in section 4, where we analyze the temperature measurements.

The application of the CFL condition implies that for the performed sequence of simulations the sampling rate is of the order of 0.5-1.0kHz. This is suitable with respect to the developing turbulence time-scales in the mixing layer. Experimental flow and temperature measurements were carried out with a sampling rate of 0.2kHz recorded for 600s. The velocity profiles were normalized with the mean bulk velocity defined as $u_b = Q/(\pi r_c^2)$, where $Q = 17.6$l/s is the mean flow rate obtained in the numerical solution, which is slightly smaller than the value obtained in the experiment. In order to obtain a global impression of the predictions obtained using the LES Vreman model, a snapshot of the temperature field is presented in Fig. 1. The temperature field $\overline{T}$ is rescaled to its nondimensional form: $T = (\overline{T} - T_c)/(T_h - T_c)$. This visual inspection is only quite crude to roughly observe turbulent structures similar to these presented in the experiment using the LIF technique. We may qualitatively observe similar flow structuring visualized by the advection of a passive scalar. Quantitative analysis will be presented momentarily.

We start our comparison of numerical and experimental results with an examination of the velocity profiles at specified locations. The comparison between application of the Smagorinsky and Vreman models was presented in (Kuczaj *et al.*, n.d.). Here we turn our attention to mesh-independent results study for the Vreman model. In order to estimate the accuracy of numerical results, several simulations with different mesh resolutions have been perfomed. Three of them, i.e., with 8mm, 4mm and 2mm average cell-size meshes are presented in Fig. 2 and Fig. 3. As can be observed, the 4mm mesh gives sufficiently accurate results in comparison to the 2mm mesh and experimental data. The 8mm mesh fails in the prediction of the mean profiles. In this case, the rms velocity fluctuations predictions are less reliable; although, they are of the similar order as for the finer meshes. It was found that differences in the results obtained on 4mm, 3mm and 2mm meshes can be practically neglected. Based on this judgement, it was concluded that the 4mm mesh provides mesh-independent results. More qualitative assessment will be given later in this section.

Profiles of the mean and fluctuations of u and w velocity components in z-direction are shown in Fig. 4-6 . These profiles are more difficult to capture, because they are strongly influenced by the mixing zone. This is particularly visible in case of fluctuations of the velocity in z-direction that is shown in Fig. 6(a). Practical estimation of an error for the fluctuations in the pipe center gives approximate value of 30% for the 8mm mesh that decreases to 15% for the 4mm mesh and reaches 5% for the 2mm mesh. Near to the wall the numerical error is decreased between results, but it is still substantial for the under-resolved simulations on the 8mm mesh. We should also notice large fluctuations of values in the presented profiles, which decrease for finer mesh resolutions. There are two reasons of such behaviour. The first one is the spatial resolution as may be expected. The second one is connected with temporal resolution that is linked with the spatial resolution through

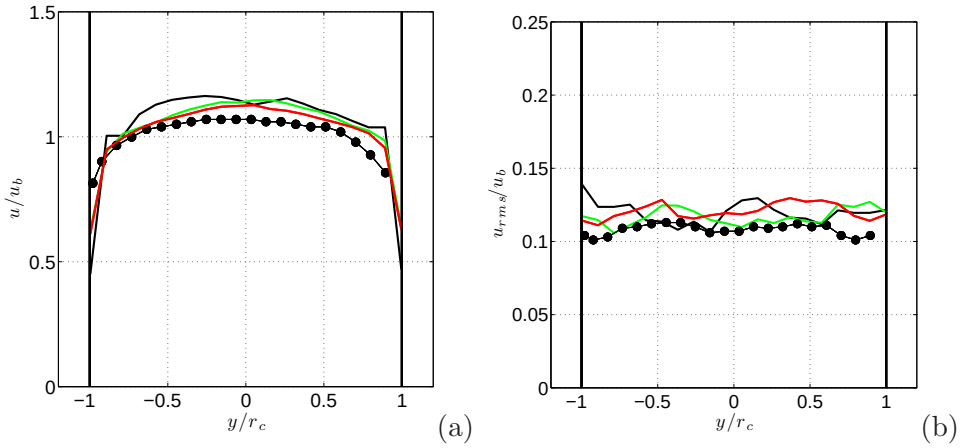

Figure 2: Time-averaged mean (a) and rms fluctuations (b) of the velocity component in x-direction. Profiles in y-direction measured at $x = 0.93$m (6.6 diameters) downstream from the center of the mixing zone. Results obtained on 8mm (black), 4mm (green), 2mm (*red*) meshes and compared with the experimental data (•).

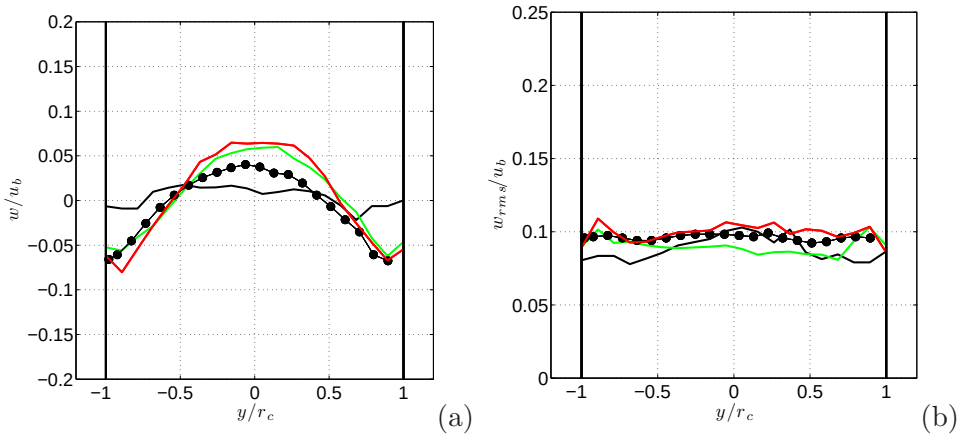

Figure 3: Time-averaged mean (a) and rms fluctuations (b) of the velocity component in z-direction. Profiles in y-direction measured at $x = 0.93$m (6.6 diameters) downstream from the center of the mixing zone. Results obtained on 8mm (black), 4mm (green), 2mm (*red*) meshes and compared with the experimental data (•).

application of the CFL stability criterion. This implies that computations are performed with a larger time-step for meshes with increased cell-sizes. Consequently, the presented time-averages are computed in the same time period of 7 seconds, but with different frequencies of recording steps. For example, for the 8mm mesh we obtain 4352 recording points, for the 4mm mesh - 8738, and for the 2mm mesh - 19482. This implicates that higher frequency events are more accurately captured on finer meshes. Two distinct approaches can be used for estimation of the numerical modelling error between various simulations in this case. The first one can be based on a practical approach, in which reporting time frequency is dictated by an optimal numerical time-stepping used in simulations. The second one implies either filtering of obtained results with the same frequency or performing simulations with the same reporting time frequency. Here we used the first aproach concentrating on numerical solutions that are obtained in practice when we usually minimize the total time of computations. We performed all simulations with a Courant number in the range of 0.7-0.85. This implies that for the 2mm mesh computations, the time-step is approximately two times smaller than in case of computations on the 4mm mesh.

Next we turn our attention to a consideration of the required mesh resolution needed to obtain mesh-independent numerical solutions. We can obtain an insight into this issue by an examination of the turbulence scales. In order to estimate the turbulence scales, we will look in detail into turbulence characteristics along the centerline of the pipe at two different measurement locations: 0.36m (2.6 diameters) and 0.93m (6.6 diameters) downstream from the center of the mixing zone.

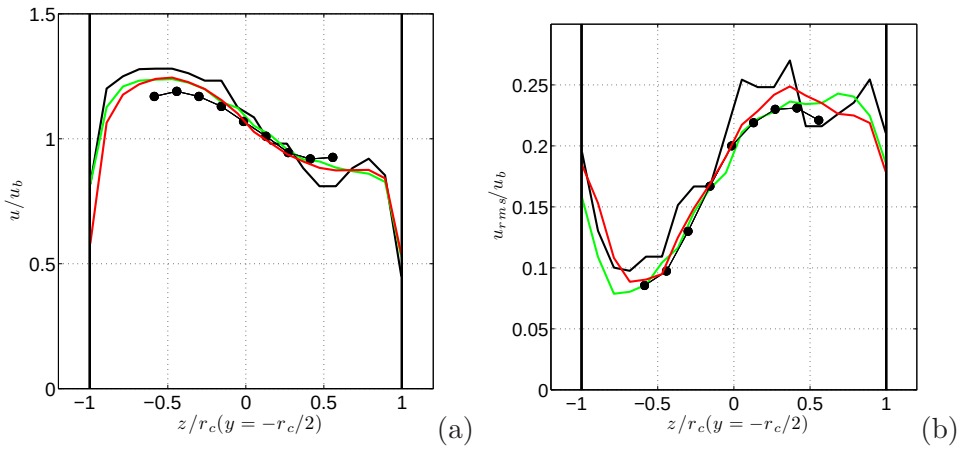

Figure 4: Time-averaged mean (a) and rms fluctuations (b) of the velocity component in x-direction at $x = 0.36$m (2.6 diameters) downstream from the center of the mixing zone. Results obtained on 8mm (black), 4mm (green), 2mm (*red*) meshes and compared with the experimental data (•).

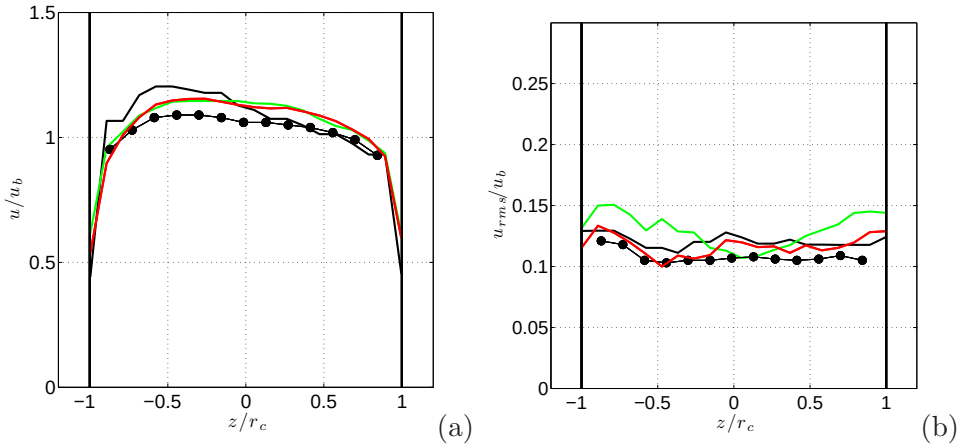

Figure 5: Time-averaged mean (a) and rms fluctuations (b) of the velocity component in x-direction at $x = 0.93$m (6.6 diameters) (bottom) downstream from the center of the mixing zone. Results obtained on 8mm (black), 4mm (green), 2mm (*red*) meshes and compared with the experimental data (•).

As we may expect, the flow at the first location still resembles the mixing zone fluctuations coming from the hot and cold fluid-streams, while at the second location turbulence is more developed. In Fig. 7(a) we present the u velocity spectra measured at the centerline $x = 0.36$m downstream of the T-junction. Results obtained for three various resolutions are compared with the experimental results recorded in the same time-span. By increasing the spatial resolution, the velocity spectra come closer to the experimental results. The Kolmogorov $-5/3$ law is shown with a solid line in Fig. 7(a) and even for the $x = 0.36$m location, which is very close to the mixing zone, a general correspondence of results can be observed. The evaluation of the rms velocity fluctuations at the centerline shows good agreement with the experimental data. On the 8mm mesh the error is approximately 30% while for the 2mm mesh is lowered below 3% (Fig. 7(b)). The natural question that can be asked is what are the resolution requirements needed to obtain mesh-independent numerical results? The general answer to this question is quite difficult, but guiding conclusions can be drawn by looking into the important turbulence time and length scales. In specific, we will look into the integral and Taylor turbulence length scales.

The computational procedure for evaluation of the turbulence scales is based on the computation of the auto-correlation coefficient from the recorded signal in time. We apply linear interpolation to the recorded velocity to obtain data distribution that is uniform in time, i.e., calculated with

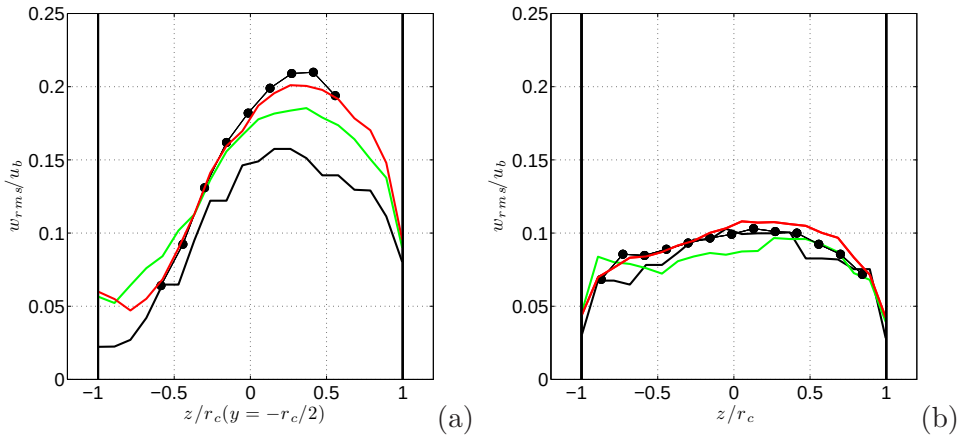

Figure 6: Time-averaged rms fluctuations of the velocity component in z-direction at $x = 0.36$m (2.6 diameters) (a) and at $x = 0.93$m (6.6 diameters) (b) downstream from the center of the mixing zone. Results obtained on 8mm (black), 4mm (green), 2mm (*red*) meshes and compared with the experimental data (•).

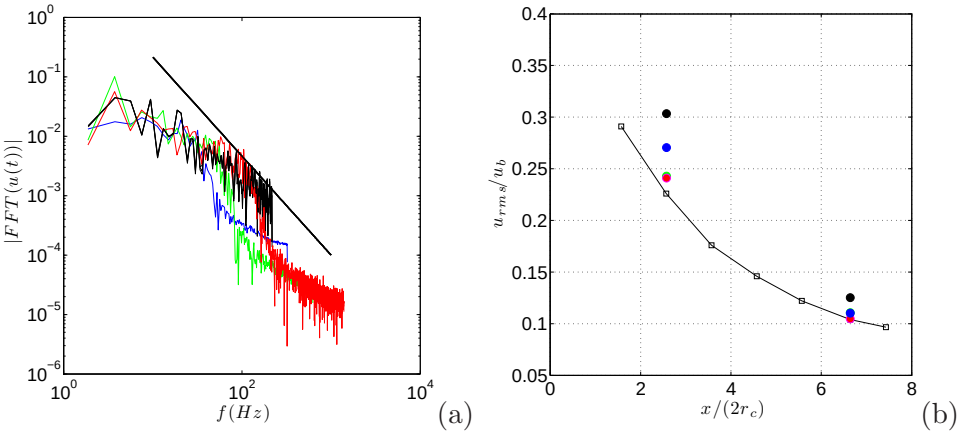

Figure 7: Streamwise velocity spectra (a) obtained on 6mm (blue), 4mm (green), 2mm (red) meshes and experimental results (black) and rms velocity (b) in x-direction obtained on 8mm (•), 6mm (•), 4mm (•), 2mm (•) meshes compared with experimental results (□).

the same reporting frequency. In the next step, we compute the auto-correlation function:

$$R(\tau) = \langle a(t)a(t+\tau)\rangle / (\langle a^2(t)\rangle^{1/2}\langle a^2(t+\tau)\rangle^{1/2}), \tag{4}$$

where $a = u(t) - \langle u(t)\rangle$, $\langle\cdot\rangle$ denotes time-averaging and τ is the separation time. The integral time scale can be then computed by integrating the correlation function: $\tau_\Lambda = \int_0^\infty R d\tau$. This procedure needs a special attention since the autocorrelation is usually non-zero for large time separation τ. The numerical procedure for computing the integral time-scale must be taken up to explicitly specified time t_k: $\int_0^{t_k} R d\tau$. As our goal is to obtain approximate estimation of the integral time-scale, another method is to apply fitting with an ad-hoc specified one-parameter function e^{τ/τ_Λ} to find the value of τ_Λ. We applied both methods for checking the consistency of two approaches finding no significant difference. For all considered cases the integral time scales are in good agreement with the maximal quantitative difference of 5%. Expanding the auto-correlation coeffcient in Taylor series about the origin we can also estimate the Taylor time-scale τ_λ (Tennekes & Lumley, 1972), which characterizes the small-scale turbulence: $R_\tau \approx 1 - \tau^2/\tau_\lambda^2$. Finally, applying the Taylor hypothesis we can estimate the Taylor microscale length: $\lambda = \overline{u}\tau_\lambda$ and the integral scale: $\Lambda = \overline{u}\tau_\Lambda$, where $\overline{u}$ is the mean value of the streamwise velocity. An example of the auto-correlation function is presented in Fig. 8(a). As we may notice, the integral length-scales τ_Λ for the 2mm mesh (red) and experimental results (black) are very similar. In Fig. 8(b) we present the Taylor

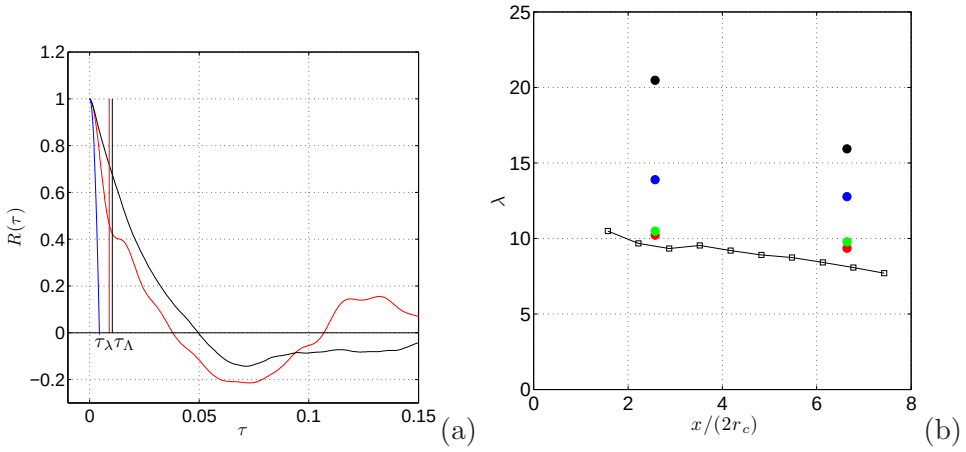

Figure 8: Auto-correlation function computed for the 2mm mesh (red) and compared with the experimental results (black) (a). Taylor microscale obtained on 8mm (•), 6mm (•), 4mm (•), 2mm (•) meshes compared with experimental results (□) (b).

microscale length for various resolutions and two different locations along the centerline, i.e., 2.6 and 6.6 diameters downstream from the center of the mixing zone. The coarsest resolution introduces an unacceptable error of the order of 100% for the estimation of λ. By improving the resolution, we come closer to the experimental results of 10mm for λ with an error of a few percent, which is close to an uncertainty in the experimental measurements. This analysis shows the importance of resolving the Taylor microscale in numerical simulations. Using the mesh cell-sizes of the order of $\lambda/3$, we can expect to obtain mesh-indpendent numerical solutions. In this case, further diminishing of the cell-sizes does not practically improve the LES results (see Fig. 7(b) and Fig. 8(b)). For average cell-sizes greater than $\lambda/3$ accuracy of the results degrades rapidly. This requirement for the minimal mesh resolution needs to be further verified in the future simulations.

4 ANALYSIS OF THE TEMPERATURE FLUCTUATIONS

In this section we turn our attention to measurements of the temperature. In both physical and numerical experiments the measurements of the temperature profiles were performed using passive scalar concentration. This does not influence the flow characteristics as the temperature is not a thermodynamical variable in this case. The profiles of the mean and rms temperature fluctuations recorded at $x = 0.93$m along the z-direction are presented in Fig. 9. At this location we still see the influence of the mixing zone, which keeps the concentration on a much higher level for positive z (influence of the hot leg). For mesh resolutions smaller than 4mm, we find a good agreement of the computational data with the experimental results. In the center of the pipe, an error of the order of a few percent is measured with a maximal value of 25% at $z/r_c = 0.5$. An average error for the rms fluctuations does not grow over 10% for the 4 and 2mm meshes. Similar conclusions can be drawn for profiles at other locations.

Further investigation of the temperature measurements at specified physical locations is presented in Fig. 10. Here, in case of the physical experiment, the measurements were performed using thermocouples. The mean temperature at seven different positions along the pipe, 1mm from the walls, correspond well with the experimental data. In general, despite the largest modelling uncertainties near to the wall, the mean values are computed with an average error of a few percent reaching maximum less than 30% at some probe locations. Similar conclusions can be drawn for the estimation of the rms fluctuations. The values are overestimated with the highest (2mm) mesh resolution. The numerical results preserve the overestimation of the fluctuations for the probes where the numerical error is significant.

It is worth to notice that for the sake of making a fair comparison between numerical and experimental data, we should apply a proper filtering of the results. Usually, the experiments provide data with a long recording time and much smaller temporal accuracy due to larger response time

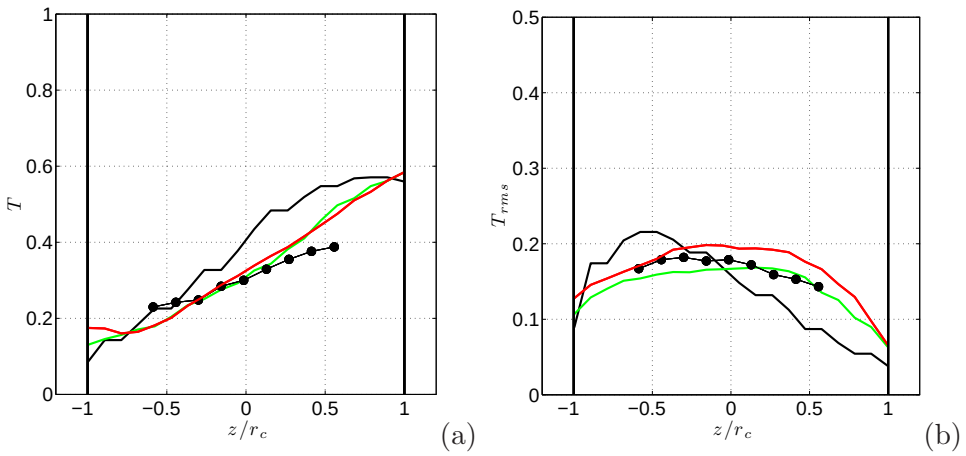

Figure 9: Time-averaged mean (a) and rms fluctuations (b) of the passive scalar concentration. Profiles at $x = 0.93$m (6.6 diameters downstream) taken along the z-direction. Results obtained on 8mm (black), 4mm (green), and 2mm (red) meshes compared with the experimental results (•).

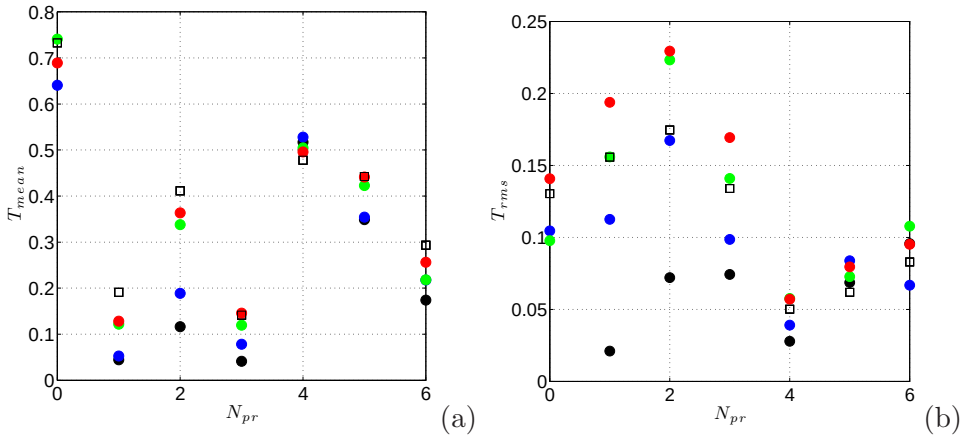

Figure 10: Time-averaged mean (a) and rms fluctuations (b) of the temperature recorded for various probe locations N_{pr}:$(x, y, z)[m]$ - 0:$(0.28, -0.005, 0.069)$, 1:$(0.28, 0.069, 0.005)$, 2:$(0.56, 0.069, 0.005)$, 3:$(0.56, 0.052, -0.045)$, 4:$(1.40, 0, 0.069)$, 5:$(1.40, 0.069, 0)$, 6:$(1.40, 0, -0.069)$. Results obtained on 8mm (•), 6mm (•), 4mm (•), 2mm (•) meshes and compared with the experimental data (□).

of the thermocouples. In case of numerical experiments this situation is reverted. The simulations are made for much shorter physical time due to high computational costs, while the reporting frequency is often dictated by the time-step of simulations, which is very small with comparison to a typical response time of the thermocouples. As a result, there is a need to check whether the simulation time is sufficient to capture the main mean flow-properties. When making comparison with experimental results we should apply filtering of data to compare them in the same frequency range. We compared the results on the 4mm mesh computed for 12s and 30s finding no significant difference. This covers the first mentioned issue. Here, we will check how the large frequency events affect fluctuations. As we already mentioned, the magnitude of fluctuations is overestimated for the finest 2mm mesh in a larger extent than for the coarser 4mm mesh. A likely reason (mentioned also in (Hu & Kazimi, 2006)), apart from the modelling error, can be linked with the recording time frequency. The reporting frequency reaches 1kHz for the 2mm mesh, while the experimental results are recorded at 0.2kHz (30 and 45Hz thermocouples) frequency. This implies that high frequency events are much better resolved using numerical simulations. In the experiment (Andersson *et al.*, 2006), it was concluded that the thermocouples with a response of 30Hz are sufficient for accurate measurements, as no significant difference was found for data recorded with thermocouples that have larger frequency. To make comparison of possible error introduced by the probing frequency in the numerical simulations, we filtered all results obtained on the 2mm and 4mm mesh. We

compared the rms values obtained without a cutoff with those filtered with a cutoff frequency of 30Hz: $\delta T_{rms}^{cfd,30Hz} = 100 * (T_{rms}^{cfd} - T_{rms}^{cfd,30Hz})/T_{mean}^{cfd}$ [%]. The same procedure was applied to experimental data. A typical temperature fluctuations recorded for 7s are shown in Fig. 11 with a corresponding spectrum filtered with a cutoff frequency of 30Hz. As the response of thermocouples was 30Hz, this procedure does not change the experimental results: $\delta T_{rms}^{exp,30Hz} \approx 0.2\%$ for all cases. Computational results are changed in the range of $\delta T_{rms}^{cfd,30Hz} \approx 1\%$ with a maximal error of 5% (see Fig. 12). It was found that for all cases this leads to smaller rms values. However, the high-frequency events have much smaller amplitude, hence they do not considerably affect the final results as it was expected. In conclusion, this provides an indication that the main source of error comes from the modelling error.

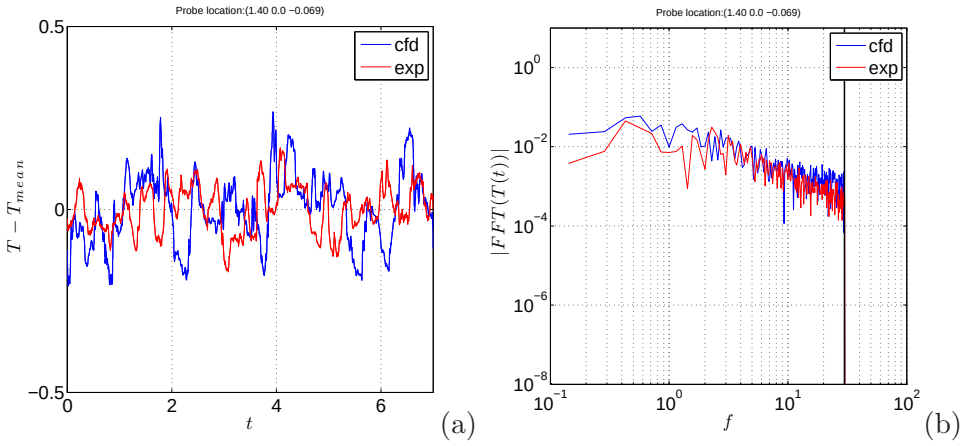

Figure 11: Temperature fluctuations computed on the 2mm mesh at the probe location N_{pr}:$(x, y, z)[m]$ - 0:$(0.28, -0.005, 0.069)$ (a). Amplitude-frequency distribution of the computational and experimental results with a cutoff frequency 30Hz (b) and recording time 7s.

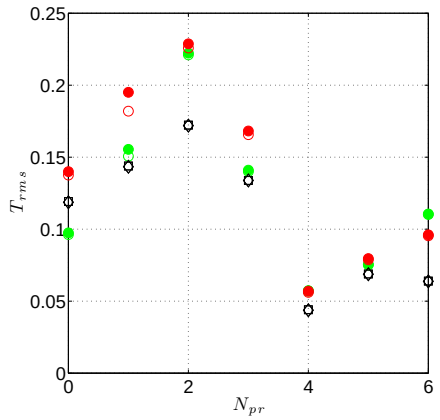

Figure 12: Time-averaged rms fluctuations of the temperature computed on the 4mm mesh (●) and 2mm mesh (●) recorded for various probe locations N_{pr} for the physical time 7s. Experimental results (□) taken also for 7s compared with the filtered results with a cutoff at 30Hz: (◇), (○), (○), correspondingly.

Finally, we consider the average and maximal error of the temperature measurements (mean and rms) obtained in the numerical simulations. It is natural to define the error for the mean temperature for each probe N_{pr} in the following way [%]:

$$\delta T_{mean}^{err} = 100 * \frac{|T_{mean}^{cfd} - T_{mean}^{exp}|}{T_{mean}^{exp}}, \tag{5}$$

and in a similar way for the rms temperature:

$$\delta T_{rms}^{err} = 100 * \frac{|T_{rms}^{cfd,30Hz} - T_{rms}^{exp}|}{T_{rms}^{exp}}. \tag{6}$$

	mean		rms	
case	avg	max	avg	max
4mm	11%	28%	7%	17%
2mm	8%	22%	11%	25%

Table 1: Average and maximal error of the computed temperature at specified probe locations on the 4mm and 2mm meshes.

This way we can compute the maximal and average mean temperature errors for all probes N_{pr}:

$$\delta T^{max}_{mean} = \max_{N_{pr}} \{\delta T^{err}_{mean}\}, \tag{7}$$

and

$$\delta T^{avg}_{mean} = \frac{1}{N_{pr}} \sum_{N_{pr}} \{\delta T^{err}_{mean}\}, \tag{8}$$

In a similar way the maximal and the average error for the rms values can be computed: δT^{max}_{rms}, δT^{avg}_{rms}. We present these errors in Fig. 13 for a number of considered probes and two computational resolutions. It is clearly seen that the finer resolution leads to the improvement of the results for the mean temperatures, but it has a reverse effect on the rms values. In this case the results on the coarser mesh have smaller error when compared to the experimental results. These results were summarized in Tab. 1, where the maximal and average mean error values are presented as defined by Eq. (7) and Eq. (8).

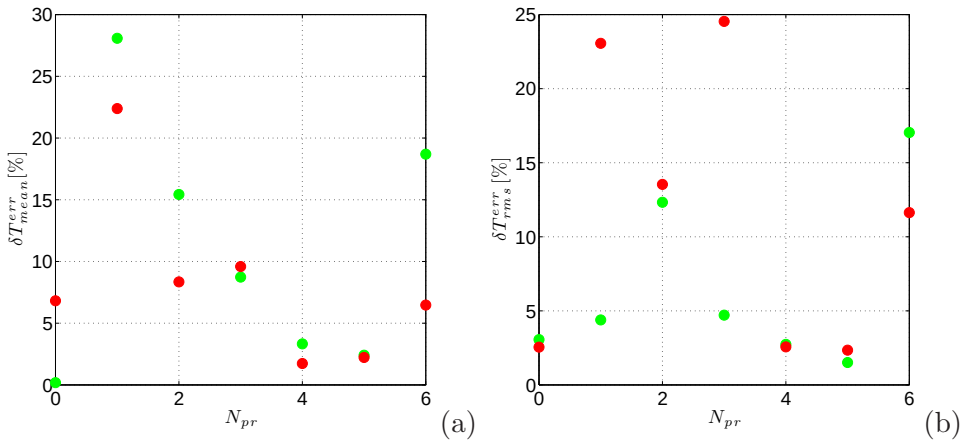

Figure 13: Mean (a) and rms (b) temperature errors for various probe locations N_{pr} obtained on the 4mm mesh (●) and 2mm mesh (●).

5 CONCLUDING REMARKS

In this paper, we studied the applicability of Large-Eddy Simulations for thermal fatigue prediction. The Vreman model was applied for LES modelling of the thermal mixing in a T-junction. Results obtained with this eddy-viscosity model were compared against experimental data. For the considered case, we found that in order to obtain mesh-independent numerical solution, the required mesh resolution must resolve the Taylor microscale length. Based on this engineering judgement, we can safely conclude that meeting this requirement allows estimating the flow characteristics with sufficient accuracy for the practical applications. Using our approach, profiles of the velocity fluctuations can be predicted with an accuracy of 5%, while the corresponding mean temperature profiles show a maximal error of 10%. This judgement is based on the velocity and temperature (LIF method for a passive scalar dye) profiles.

For thermal fatigue the main objective is to accurately predict fluctuations of the flow variables near to the wall. Analysis of temperature fluctuations recorded at various spatial probe locations (thermocouples 1mm from the wall), shows that LES provides overestimations of magnitude of the fluctuations. We have checked the possibility for an error coming from the distinct reporting frequencies that exist in the numerical and physical experiments. Performing comparison of filtered data with a cutoff frequency 30Hz, we found that this procedure does not significantly change the obtained results. Maximal error introduced this way reaches 5% at some probe locations. The average and mean errors in the estimation of the temperature at specified probe locations are reported in Table 1. This judgement is based on the comparison with the experimental data taken from the thermocouples measurements at specified spatial locations. By performing simulations on a sequence of mesh resolutions, we conclude that the main source of the error comes from the modelling.

References

Andersson, U., Westin, J., & Eriksson, J. 2006. *Thermal mixing in a T-junction.* Tech. rept. U 06-66. Vattenfall Research and Development AB.

Chapuliot, S., Gourdin, C., Payen, T., Magnaud, J.P., & Monavon, A. 2005. Hydro-thermal-mechanical analysis of thermal fatigue in a mixing tee. *Nuclear Engineering and Design*, **235**, 575 – 596.

Coste, P., Quemere, P., Roubin, P., Emonot, P., Tanaka, M., & Kamide, H. Large Eddy Simulation of a mixing-T experiment. *In: ICAPP Proceedings, June 4-8, 2006, Reno, NV, USA.*

Fureby, C., Tabor, G., Weller, H., & Gosman, A.D. 1997. A Comparative Study of Sub-Grid Scale Models in Homogeneous Isotropic Turbulence. *Phys. Fluids*, **9**(5), 1416 – 1429.

Hu, L.-W., & Kazimi, M.S. 2006. LES benchmark study of high cycle temperature fluctuations caused by thermal striping in a mixing tee. *Int. J. Heat and Fluid Flow*, **27**, 54 – 64.

Kuczaj, A.K., de Jager, B., & Komen, E.M.J. An assessment of Large-Eddy Simulation for thermal fatigue prediction. *In: ICAPP Proceedings, June 8-13, 2008, Anaheim, California, USA.*

Merzari, E., & Ninokata, H. Test of Large Eddy Simulation Sub-Grid-Scale models for flows in annular channels. *In: ICAPP Proceedings, May 13-18, 2007, Nice, France.*

Tennekes, H., & Lumley, J.L. 1972. *A first course in turbulence.* MIT Press.

Vreman, A.W. 2004. An eddy-viscosity subgrid-scale model for turbulent shear flow: algebraic theory and applications. *Phys. Fluids*, **16**(10), 3670 – 3681.

Weller, H.G., Tabor, G., Jasak, H., & Fureby, C. 1998. A tensorial approach to computational continuum mechanics using object orientated techniques. *Comput. Phys.*, **12**(6), 620 – 631.

Westin, J., 't Mannetje, C., Alavyoon, F., Veber, P., Andersson, L., Andersson, U., Eriksson, J., Henriksson, M., & Andersson, C. High-cycle thermal fatigue in mixing tees. Large-eddy simulations compared to a new validation experiment. *In: ICONE Proceedings, May 11-15, 2008, Orlando, Florida, USA.*